RSC Advances

PAPER

View Article Online
View Journal | View Issue

Cite this: *RSC Adv.*, 2021, **11**, 21607

Nitrogen and sulfur Co-doped carbon dots as ecofriendly and effective corrosion inhibitors for Q235 carbon steel in 1 M HCl solution

Mingjun Cui *[a] and Xia Li[b]

Received 9th April 2021
Accepted 1st June 2021

DOI: 10.1039/d1ra02775a

rsc.li/rsc-advances

Novel nitrogen and sulfur co-doped carbon dots (N,S-CDs) were synthesized *via* a hydrothermal procedure using citric acid (CA) and thiourea (TU) as precursors, and the corresponding corrosion protection performance was first investigated for Q235 carbon steel in 1 M HCl solution. Experimental results indicated that N,S-CDs as mixed-type corrosion inhibitors could effectively prevent Q235 carbon steel from corrosion in 1 M HCl solution, and the corrosion inhibition efficiency was improved with the increase in N,S-CD concentration. The maximum value was achieved at 400 ppm of N,S-CDs at 25 °C, which was approximately 96.6%, 94.6% and 90.55%, according to the potentiodynamic polarization curves, EIS results and weight loss measurement, respectively. Additionally, with the temperature ranging from 25 to 55 °C, the inhibition efficiency obtained from the weight loss measurement was enhanced from 90.55% to 94.04%. Such superior inhibition effect was assigned to the physisorption and chemisorption of N,S-CDs on the Q235 carbon steel surface, which was also be confirmed by XPS analysis. The adsorption of N,S-CDs onto a steel substrate conformed to the Langmuir adsorption isotherm.

1. Introduction

Carbon steel, as one of the structural materials widely applied for engineering and daily life, is extremely sensitive to aggressive solutions, which makes it highly susceptible to corrosion during the pickling process.[1,2] To effectively suppress the corrosion of carbon steel in harsh environments to an acceptable range, organic inhibitors with heteroatoms (*e.g.*, nitrogen, oxygen and sulfur), polar functional groups, and/or multiple bonds are generally employed.[3–5] However, as their effects on human health, ecology and environment are of great concern, it is urgent to develop effective, safe and eco-friendly corrosion inhibitors. It has been proved that natural extracts from longan seeds,[6] fruits,[7] flowers[8] and so on can be used as effective corrosion inhibitors to prevent metal corrosion, but large amounts of organic solvents may be needed for the extracting processes, leading to a huge amount of wastes.

Since the discovery of carbon dots (CDs), sustainable attention has been paid to them owing to their outstanding properties, *e.g.*, excellent water solubility, hypotoxicity, stable chemical properties, and good biocompatibility.[9–11] Such unique performance makes them applicable in the fields of biosensors, bioimaging, catalysis, and drug delivery. In addition, CDs have also begun to be used as corrosion inhibitors to retard metal corrosion in acidic solutions. Cui *et al.* found that nitrogen-doped CDs (NCDs) prepared with antibiotic aminosalicylic acid (ASA) or *p*-phenylenediamine (*p*-PD), or *o*-phenylenediamine (*o*-PD) could effectively suppress corrosion of Q235 carbon steel in 1 M HCl solution, exhibiting a high inhibition efficiency up to 90%.[12,13] Subsequently, it was found that these NCDs could also provide excellent protection for Cu at a temperature of 298–318 K in 0.5 M H_2SO_4 solution.[14] Besides, Ye *et al.* prepared various types of NCDs with different source materials and investigated their corrosion inhibition performance.[15–17] NCDs exhibit superior inhibition performance because N atoms with strong electronegativity and electron-donating capability could interact with the steel surface *via* physisorption and chemisorption to form a protective NCD film. Until now, most of the investigations have focused on the corrosion inhibition by single-element doped CDs for Q235 carbon steel in acid solutions, while dual-element co-doped CDs have been rarely studied. It had been demonstrated by Denis *et al.* that dual doping of N and S atoms was more effective to improve the reactivity of graphene and contributed to adsorption between graphene and metals (K, Na and Li).[18–21] Thus, it can be anticipated that dual doping of N and S in CDs (N,S-CDs) may also be beneficial for their adsorption on Fe, thus inhibiting the corrosion of metals. Recently, Yadav *et al.* have prepared two kinds of carbon dots by solvothermal treatment (N,S-CDs: pyromellitic acid, thiourea and DETA; N-CDs: pyromellitic acid, urea and DETA), and the results indicated that N,S-CDs exhibited higher inhibition efficiency (96.4%) than N-CDs

[a]*Key Laboratory of Impact and Safety Engineering, Ministry of Education, School of Mechanical Engineering and Mechanics, Ningbo University, Ningbo, 315211, China. E-mail: cuimingjun@nbu.edu.cn*

[b]*State Key Laboratory of Solid Lubrication, Lanzhou Institute of Chemical Physics, Lanzhou 730000, China*

(90%) at 100 ppm and 303 K. This result indicates that dual doping of S and N atoms in carbon dots is more effective to inhibit the corrosion of metals than single doping of N atom.[22] Meanwhile, Chen and coworkers found that N,S-CDs could effectively prevent the corrosion of carbon steel in 3.5 wt% NaCl solution with saturated CO_2, realizing a inhibition efficiency of about 93% at 50 ppm.[23] Furthermore, the addition of N,S-CDs could also effectively suppress the corrosion of 5052 aluminium alloy in 0.1 M HCl solution, and the inhibition efficiency was up to 85% at 5 ppm.[24] Nevertheless, the investigated corrosive medium is relatively mild with respect to the industrial pickling process of metals, and it is unknown whether N,S-CDs can still effectively inhibit the metal corrosion under more harsh environments.

Hence, in this study, N,S-CDs were prepared by a hydrothermal method with citric acid monohydrate ($CA \cdot H_2O$) and thiourea as precursors. The synthesized N,S-CDs were characterized using scanning probe microscopy (SPM), X-ray photoelectron spectroscopy (XPS), Fourier transform infrared (FTIR) and ultraviolet-visible (UV-vis) spectroscopy. The corrosion behavior of Q235 carbon steel in 1 M HCl solution with different concentrations of N,S-CDs was evaluated by electrochemical impedance spectroscopy (EIS), potentiodynamic polarization tests and weight loss measurement, exhibiting a high inhibition efficiency of 96.6%. Furthermore, the surface morphology and chemical information of the corroded steel were analyzed to reveal the possible inhibition mechanism of N,S-CDs. The aim of this work is to propose a novel N,S-CD inhibitor to retard metal corrosion and reveal its inhibition mechanisms in an attempt to extend its application in harsh engineering environments.

2. Experimental method

2.1 Materials

Citric acid monohydrate ($CA \cdot H_2O$) and thiourea were purchased from Aladdin (Shanghai, China) and Macklin Biochemical Co., Ltd (Shanghai, China), respectively. Concentrated hydrochloric acid (HCl, 37%, AR) was provided by Sinopharm Chemical Reagent Co., Ltd (Shanghai, China), and 1 M HCl solution was prepared by diluting 37% HCl with distilled water. The test solutions with different concentrations of N,S-CDs were prepared by adding a certain amount of N,S-CD powder and 1 M HCl solution in a volumetric flask. Q235 carbon steel substrates ($20 \times 40 \times 3$ mm^3) were used as the tested electrode. Prior to the test, Q235 carbon steel was degreased with acetone and alcohol successively, mechanically polished using 400 and 800 grit of abrasive papers, washed ultrasonically with alcohol, and finally, dried at room temperature.

2.2 Synthesis of N,S-CDs

In the work, N,S-CDs were prepared by a hydrothermal synthesis method according to a previous report.[25] Citric acid (0.3 g) and thiourea (0.6 g) were dissolved into 5 mL of deionized water under ultrasonication, and then, the mixture was transferred into a polytetrafluoroethylene autoclave. Afterward, the autoclave was placed into an oven and heated from room

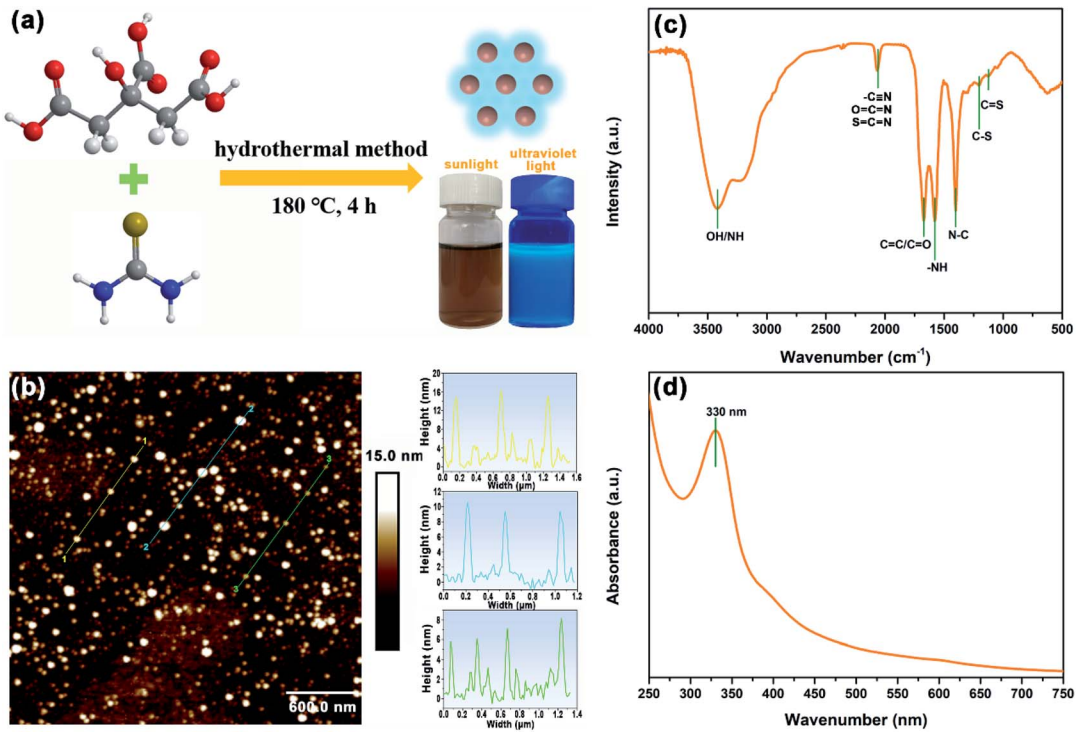

Fig. 1 (a) Preparation of N,S-CDs, (b) SPM image of N,S-CDs and the height profiles along the corresponding lines, (c) FTIR spectrum and (d) UV-vis spectrum of N,S-CDs.

temperature to 180 °C, maintained at 180 °C for 4 h, and finally, cooled down naturally to room temperature. The obtained dark brown mixtures were refined using a dialysis bag (molecular weight cut-off ~ 500 Da) for 24 h to remove the unreacted chemicals. Finally, rotary evaporation technique was used to remove the residual water, and the obtained products were further dried in a vacuum oven for 24 h.

2.3 Characterization of N,S-CDs

A scanning probe microscope (SPM, Veeco Dimension 3100V, America) was used to check the morphology and size of N,S-CDs. Fourier transform infrared (FTIR, America) spectra were recorded using a Nicolet 6700 FTIR spectrometer over the wavenumber of 500–4000 cm^{-1}. UV-vis absorption spectra were recorded using a Lambda 950 UV-Vis spectrophotometer (America). The elemental composition and chemical bonding of N,S-CDs were examined using an X-ray photoelectron spectrometer (XPS, AXIS ULTRA DLD, England).

2.4 Electrochemical tests

Electrochemical tests were performed using a CHI760e electrochemical workstation with a conventional three-electrode

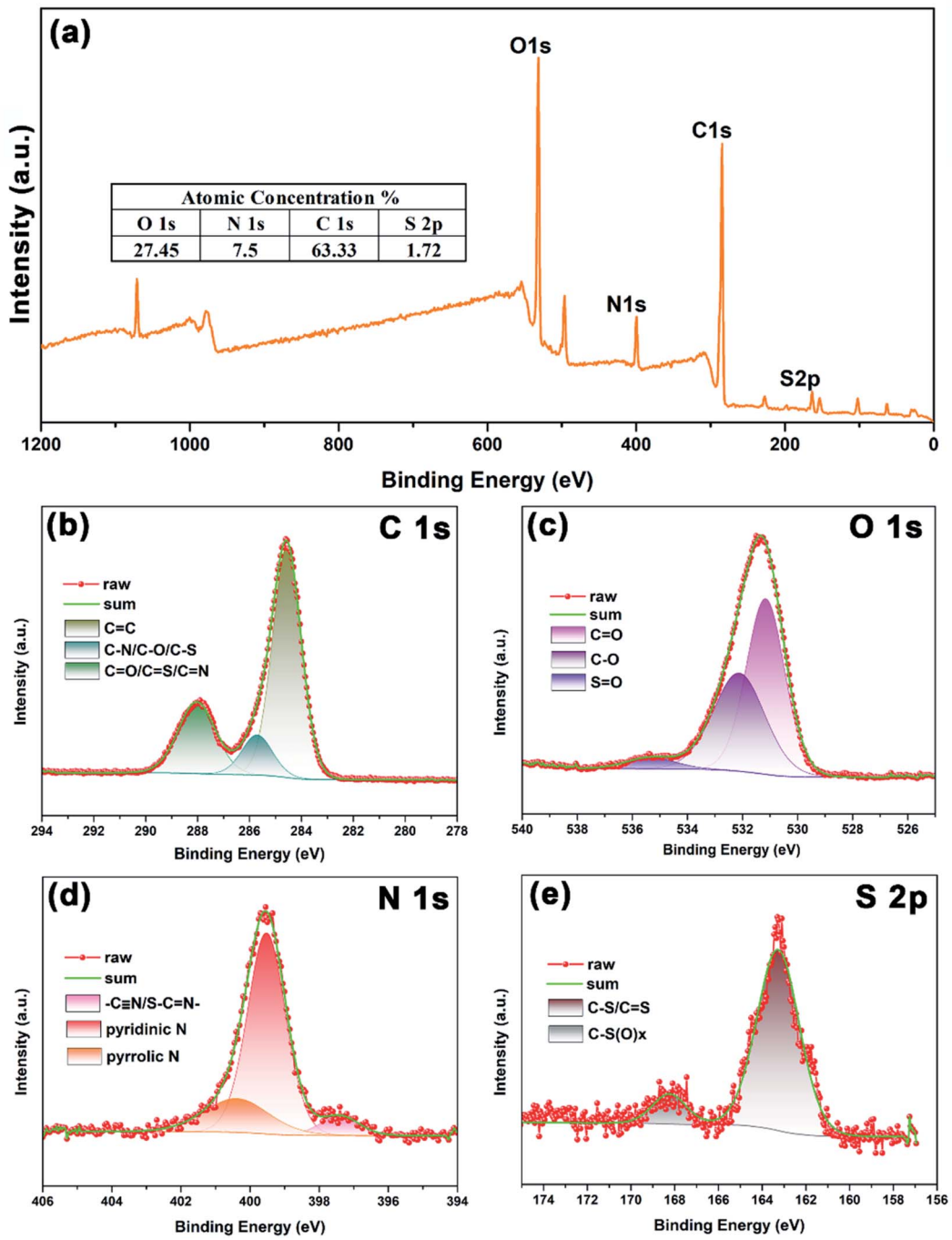

Fig. 2 (a) XPS survey spectrum of N,S-CDs, and high-resolution spectra for (b) C 1s, (c) O 1s, (d) N 1s, and (e) S 2p.

system consisting of a saturated Ag/AgCl electrode (reference electrode), a platinum sheet (auxiliary electrode) and a Q235 carbon steel substrate (1 cm^2 of exposure area, working electrode). Prior to the electrochemical impedance spectroscopy (EIS) test, open circuit potential (OCP) test was measured until the system reached a steady state. Subsequently, the EIS test was performed at OCP over the frequencies ranging from 100 kHz to 10 mHz, with 5 mV of disturbance signal. Then, the EIS results were analyzed using the Zsimpwin 3.21 software. In case of the potentiodynamic polarization tests, experimental scanning was performed at a potential ranging from −250 mV to 250 mV relative to OCP with a scanning rate of 0.5 mV s^{-1}.

2.5 Weight loss measurement

Weight loss measurement was performed by immersing Q235 carbon steel substrates (10 × 10 × 1 mm^3) in the tested solutions. Prior to the measurement, each specimen was weighed thrice using an analytical balance. After different time intervals, the specimens were taken out, washed with distilled water, dried and reweighed accurately. Finally, the average mass of specimen at different immersion time points was used for calculating the corrosion rates.

2.6 Surface analysis

After the weight loss measurement, the specimens were taken out, washed, and dried in a vacuum oven. Then, the surface morphology and surface roughness of specimens were examined using a scanning electron microscope (SEM, Hitachi, SU5000) and a laser scanning confocal microscope (LSCM, Zeiss, LSM700, Germany), respectively. To further reveal the corrosion inhibition mechanism of N,S-CDs, the elemental composition and surface bonding state of specimens were checked by XPS.

3. Results and discussions

3.1 Characterization of N,S-CDs

The synthesis of N,S-CDs was realized by heating CA.H_2O and TU in water at 180 °C for 4 h. As shown in Fig. 1a, the obtained products are homogeneously dispersed into water to form a brown color at sunlight and blue fluorescence under the illumination of UV (365 nm). Subsequently, the morphology and size of N,S-CDs were characterized by SPM. It can be seen from Fig. 1b that N,S-CDs show a spherical feature with different sizes ranging from 6 to 16 nm. The chemical structure of N,S-CDs was checked by FTIR. As illustrated in Fig. 1c, the broad peak at 3422 cm^{-1} corresponds to O–H and N–H. The characteristic absorption peak of cumulated double bonds can be observed at 2065 cm^{-1}, which is assigned to C≡N, N=C=S and N=C=O.[23,26,27] The peak at 1672 cm^{-1} is attributed to the stretching vibrations of C=N and C=O. The peaks for the bending vibration of N–H and the stretching vibration of C–N can be observed at 1578 cm^{-1} and 1400 cm^{-1}, respectively.[28]

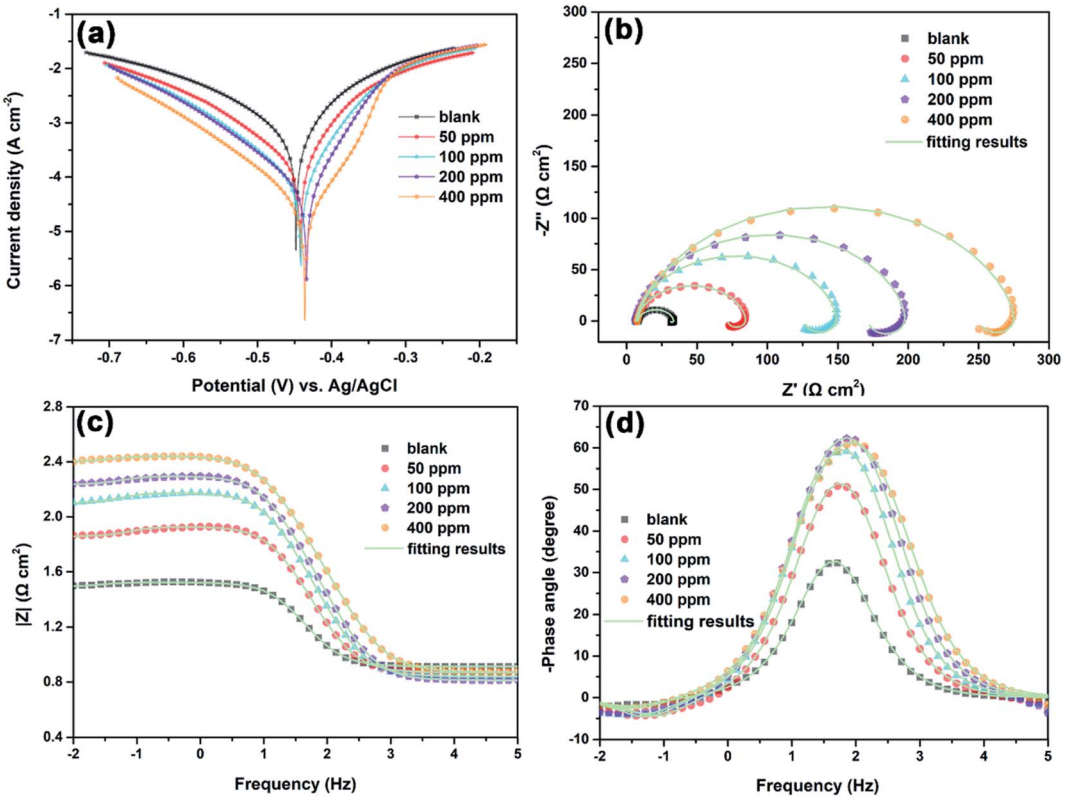

Fig. 3 (a) Polarization and (b–d) EIS curves of Q235 carbon steel in 1 M HCl solution with and without different concentrations of N,S-CDs at room temperature.

The peaks at 1200 and 1128 cm^{-1} are assigned to C–S and C═S, respectively.[23,29] As indicated by UV-vis absorption spectrum in Fig. 1d, an apparent absorption peak at *ca.* 330 nm can be attributed to n–π* transition associated with both heteroatom doping and surface functionalization of carbon core.[27] Hence, a bright blue fluorescence can be observed when N,S-CDs are dispersed in water under UV irradiation at 365 nm (inset in Fig. 1a).

To research the elemental composition and surface bonding states of N,S-CDs, XPS technique was employed and the corresponding results are shown in Fig. 2. XPS survey spectrum of N,S-CDs in Fig. 2a shows four peaks centered at around 163, 285, 400 and 532 eV, which are attributed to the presence of S 2p (1.7 at%), C 1s (7.5 at%), N 1s (27.4 at%) and O 1s (63.3 at%). This result indicates the successful incorporation of S and N atoms into the CDs. The high-resolution spectrum of C 1s can be divided into three peaks located at 284.6, 285.7 and 288 eV, which are associated with the sp^2 C (C═C), sp^3 C (C–N, C–O and C–S), and C═O/C═S/C═N, respectively (Fig. 2b).[30,31] The deconvolution of O 1s shows three peaks centered at 531.2, 532 and 535.4 eV, which correspond to C═O, C–O and S═O, respectively (Fig. 2c). The N 1s spectrum shown in Fig. 2d exhibits three peaks at 397.3, 399.5 and 400.4 eV, suggesting the existence of –C═N/S═C═N–, pyridinic N and pyrrolic N. The appearance of the peak at 397.3 eV (–C═N/S═C═N–) is in accordance with the FTIR results in Fig. 1c. In case of S 2p spectrum, two peaks located at 163.3 and 168.3 eV are attributed to the presence of C–S/C═S and C–SO_x, respectively (Fig. 2e).[10,30,32]

3.2 Electrochemical measurements

Potentiodynamic polarization curves of Q235 carbon steel in 1 M HCl solution with and without different concentrations of N,S-CDs are presented in Fig. 3a, and the corresponding electrochemical parameters and inhibition efficiency (η) are listed in Table 1. The inhibition efficiency was calculated according to the following equation:[33,34]

$$\eta = \frac{i^0_{corr} - i_{corr}}{i^0_{corr}} \times 100 \quad (1)$$

where η is the inhibition efficiency, and i^0_{corr} and i_{corr} correspond to the corrosion current density with and without N,S-CDs, respectively.

It can be observed from Table 1 that the corrosion current density (i_{corr}) reduces pronouncedly and the corrosion potential (E_{corr}) shows a slightly positive shift with the increase in N,S-CDs concentration. The negligibly positive shift of E_{corr} implies that the inhibitory effect of N,S-CDs is achieved mainly by the geometric blocking effect.[25] Besides, both anodic dissolution and cathodic reduction reaction are inhibited apparently after the addition of N,S-CDs in 1 M HCl solution, and the anodic reaction is prevented more effectively. Meanwhile, the inhibition efficiency increases with the increase in N,S-CD concentration. The above-mentioned results indicate that N,S-CDs can act as a mixed-type inhibitor. For the cathodic part of polarization curves, nearly parallel polarization curves indicate that the cathodic reaction is still controlled by proton reduction mechanism.[35] However, N,S-CDs can be adsorbed onto the Q235 carbon steel surface to block the active sites, thus effectively inhibiting the cathodic reduction reaction. In case of the anodic branch of polarization curves, the i_{corr} decreases obviously when the potential is lower than −0.33 V (*vs.* Ag/AgCl), indicating the formation of a protective N,S-CDs film on the steel surface under such conditions. Once the polarization potential is higher than −0.33 V (*vs.* Ag/AgCl), the anodic current density in the presence of N,S-CDs turns into coincidence with that in a blank solution because of the desorption of N,S-CDs from the steel surface.[23]

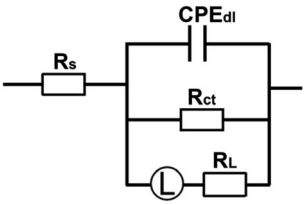

Fig. 4 Equivalent circuit used to fitting the EIS results in Fig. 3.

The EIS test was used to evaluate the corrosion behavior of Q235 carbon steel in 1 M HCl solution with and without different concentrations of N,S-CDs after 3 h of immersion at room temperature. As shown in Fig. 3b, whether N,S-CDs exist or not, Nyquist plots of all specimens exhibit a depressed capacitive arc at high and medium frequencies corresponding to the charge transfer process, and the depressed shape of capacitive arc is caused by the surface inhomogeneity and roughness of the specimen.[6,35] In addition, an inductive loop can also be observed at low frequencies owing to the adsorption of intermediate products.[6,36,37] The diameter of the capacitive arc increases with the increase in N,S-CD concentration, revealing that the addition of N,S-CDs can retard the charge transfer process and improve the inhibition efficiency. The

Table 1 Electrochemical parameters obtained from polarization curves for Q235 carbon steel in 1 M HCl with and without different concentrations of N,S-CDs

C (ppm)	E_{corr} (mV)	i_{corr} (μA cm^{-2})	β_c (mV dec^{-1})	β_a (mV dec^{-1})	η%
Blank	−448	657	−138.2	128.4	—
50	−445	184	−111.1	69.0	72
100	−441	87.7	−101.4	54.8	86.6
200	−434	56.7	−101.4	50.5	91.4
400	−436	22.3	−101.9	49.0	96.6

Table 2 Electrochemical parameters obtained from EIS results for Q235 carbon steel in 1 M HCl solution with and without different concentrations of N,S-CDs

			CPE_{dl}					
C (ppm)	R_s (Ω cm^2)	R_{ct} (Ω cm^2)	$Y_0 \times 10^5$ (Ω^{-1} cm^{-2} s^n)	n	C_{dl} (μF cm^{-2})	L (H cm^2)	R_L (Ω cm^2)	η (%)
Blank	8.16	25.28	46.6	0.91	261.00	1375	239	—
50	6.40	77.73	19.2	0.92	109.00	873.5	385.5	81.3
100	6.92	143.1	13.2	0.92	73.30	2310	723.4	89.8
200	6.48	192.9	10.8	0.91	54.01	3614	1161	92.5
400	6.44	270	9.18	0.88	32.40	1.07×10^4	2511	94.6

corresponding Bode plots of Q235 carbon steel in 1 M HCl solution with and without different concentrations of N,S-CDs are presented in Fig. 3c and d. The impedance modulus at 0.01 Hz increases with the increase in N,S-CD concentration, and the maximum impedance modulus is about $10^{2.4}$ Ω cm^2 in the presence of 400 ppm N,S-CDs, which is nearly eight times larger than that in the blank solution. According to the shape of all Bode-phase plots, there is one single peak at the high and medium frequencies, which corresponds to the electrical double layer. Moreover, the phase angle becomes more negative with the increase in N,S-CD concentration, signifying that more N,S-CDs are adsorbed onto the steel surface as the N,S-CD concentration increases. It is worth noting that all EIS plots display similar shapes regardless of the absence and presence of N,S-CDs, indicating that the introduction of N,S-CDs into a HCl solution does not change the electrochemical reaction mechanism and just inhibits the charge transfer process by adsorbing onto the steel surface to form a protective layer.

According to the above-mentioned EIS results, the equivalent circuit shown in Fig. 4 is proposed to fit the EIS results. In the equivalent circuit, R_s is the solution resistance, and R_{ct} and CPE_{dl} correspond to the charge-transfer resistance and the double layer capacitance, respectively. R_L and L stand for the inductive resistance and inductance, respectively. The use of CPE rather than the ideal capacitor is owing to the inhomogeneity of the surface. According to the previous reports, the value of the double layer capacitance (C_{dl}) could be calculated based on Brug's formula in eqn (2).[14,38]

$$C_{dl} = Y_0^{\frac{1}{n}}\left(\frac{1}{R_s} + \frac{1}{R_{ct}}\right)^{(n-1)/n} \quad (2)$$

where Y_0 is the magnitude of CPE and n corresponds to a phase shift ($-1 \le n \le 1$).

The fitting electrochemical parameters obtained from EIS results are summarized in Table 2, where the R_{ct} value increases from 25.28 Ω cm^2 to 270 Ω cm^2, and the C_{dl} value decreases with the increase in N,S-CD concentration. The decrease in the C_{dl} value is ascribed to the bonding of N,S-CDs with the active sites on steel surface instead of hydrogen bonding with water molecules.[39] Furthermore, the inhibition efficiency was calculated using the following equation:[6,17,40]

$$\eta = \frac{R_{ct} - R_{ct}^0}{R_{ct}} \times 100\% \quad (3)$$

where R_{ct}^0 and R_{ct} correspond to the charge transfer resistance in the absence and presence of N,S-CDs, respectively. It can be observed from Table 2 that the inhibition efficiency is significantly improved with the increase in N,S-CD concentration and the highest inhibition efficiency is approximately 94.6% at 400 ppm N,S-CDs, which agrees well with those in Table 1.

3.3 Effect of immersion time

Weight loss measurement as a reliable and simplest approach was employed to determine the corrosion rate of Q235 carbon steel in the tested solutions as well as the inhibition efficiency

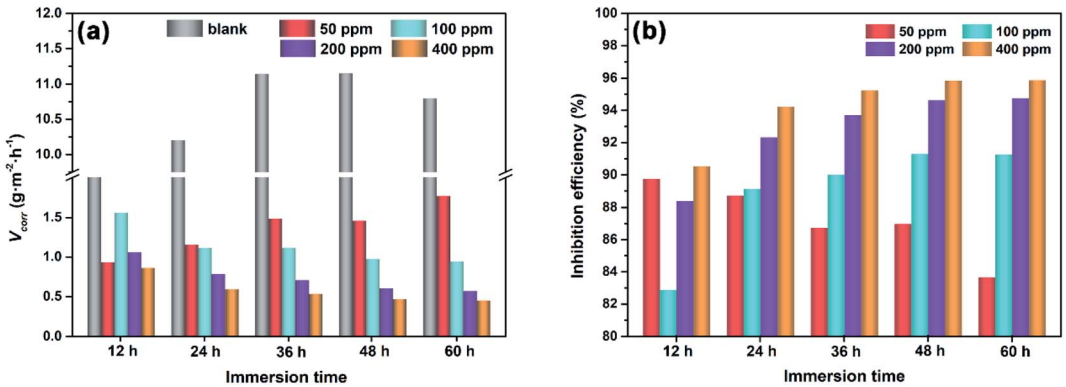

Fig. 5 (a) Corrosion rate and (b) inhibition efficiency for Q235 carbon steel during 60 h of immersion in 1 M HCl without and with different concentrations of N,S-CDs.

of N,S-CDs, in which the corrosion rate (V_{corr}) and the inhibition efficiency can be obtained according to the following equations:

$$V_{corr} = \frac{m_0 - m_t}{At} \quad (4)$$

$$\eta = \frac{V^0_{corr} - V_{corr}}{V^0_{corr}} \times 100 \quad (5)$$

where V^0_{corr} and V_{corr} are the corrosion rate in the tested solution without and with N,S-CDs, respectively. m_0 is the initial mass (g) of specimens prior to immersion, t is the immersion time (h), m_t is the mass (g) of specimen after t h of immersion, and A is the exposed area (m^2) of specimen.

As displayed in Fig. 5, the V^0_{corr} value in blank solution ranges from 9.1 to 11.1 g m^{-2} h^{-1} during 60 h of immersion. In the presence of N,S-CDs, the corrosion rate of Q235 carbon steel decreases remarkably compared to that in the blank solution. Under 50 ppm N,S-CDs, the V_{corr} value increases from 0.9 to 1.8 g m^{-2} h^{-1} and the inhibition efficiency decreases from 89.74% to 83.65% with the prolonged immersion time. When the N,S-CD concentration is equal to or higher than 100 ppm, the V_{corr} value decreases and inhibition efficiency increases with the increase in N,S-CD concentration and immersion time, *i.e.*, the minimum V_{corr} (0.45 g m^{-2} h^{-1}) and maximum inhibition efficiency (95.86%) are achieved after 60 h of immersion in 1 M HCl with 400 ppm N,S-CDs. This is a clear demonstration of the high inhibitory effect of N,S-CDs, which is due to the strong adsorption interaction between N,S-CDs molecules and the steel surface.

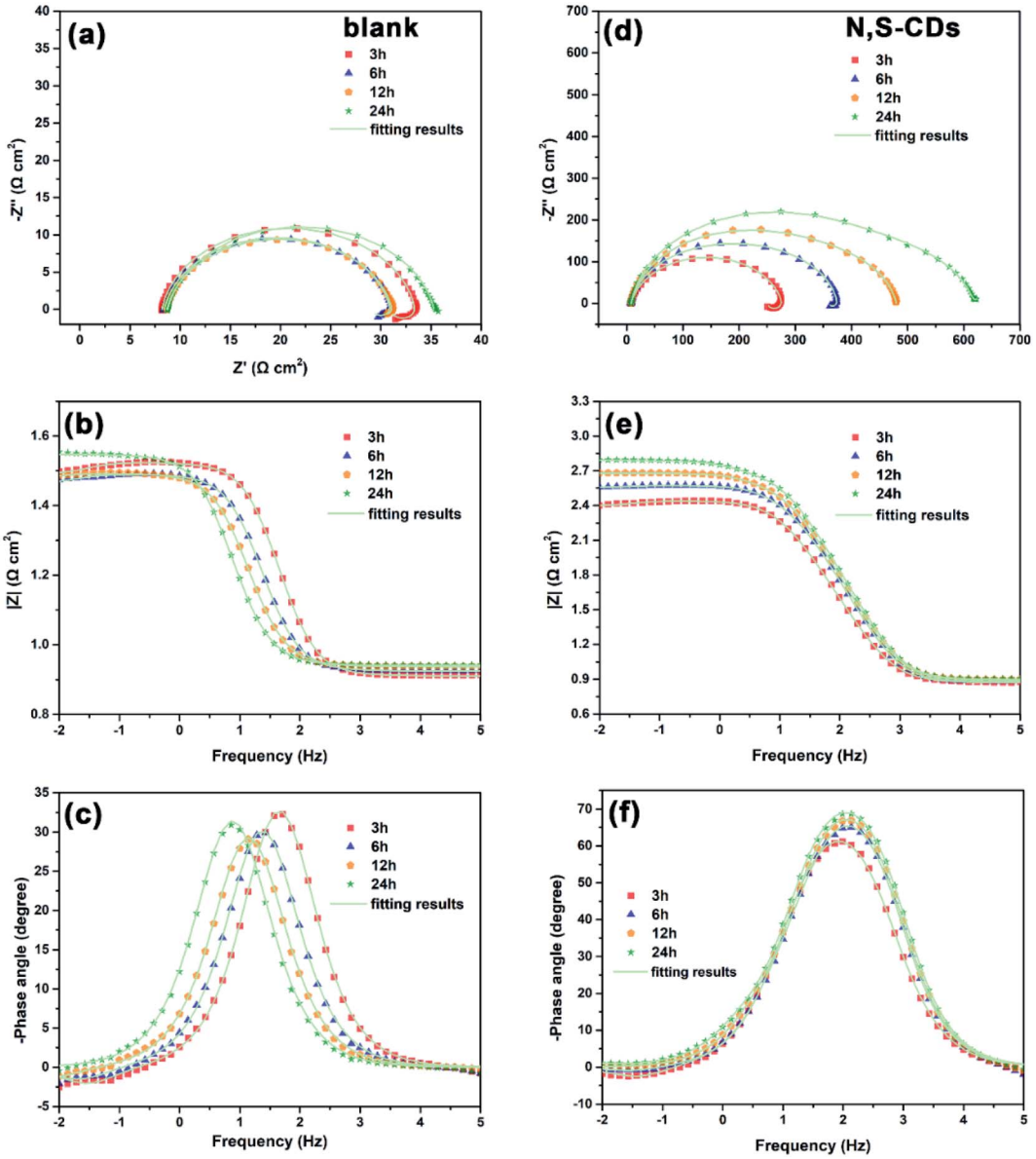

Fig. 6 Variation in the EIS curves of Q235 carbon steel after different immersion time points in 1 M HCl solution without (a–c) and with (d–f) 400 ppm of N,S-CDs at room temperature.

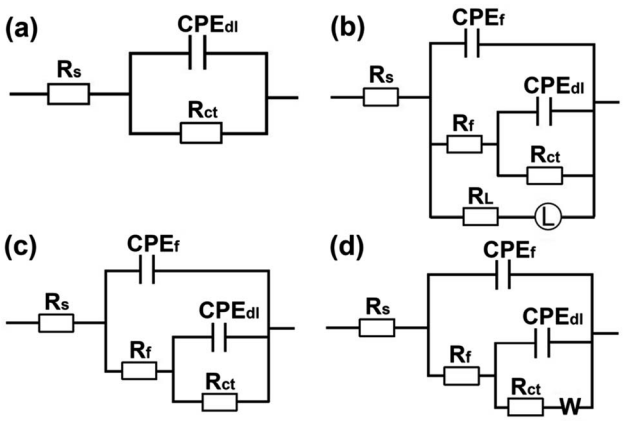

Fig. 7 Equivalent circuits used for fitting EIS data at different immersion time points, (a) 24 h in blank solution, (b) 6 h, (c) 12 h, and (d) 24 h in 400 ppm N,S-CDs.

In order to deeply understand the corrosion behavior of Q235 carbon steel with the increase in immersion time, EIS measurements were carried out in 1 M HCl with and without 400 ppm N,S-CDs for a duration of 24 h. It is apparent from Fig. 6a that the Nyquist plots in blank solution during 12 h of immersion show a depressed capacitive arc and an inductive loop, and only one time constant exists in the phase angle-Bode plots. Hence, the equivalent circuit in Fig. 4 is still available for fitting the EIS data before 12 h of immersion. With the extension of immersion time, the diameter of capacitive arc and the impedance modulus in Bode plots vary slightly (Fig. 6a and b), while the inductive loop disappears at 24 h of immersion because of the formation of corrosion products. Thus, the inductive elements in Fig. 4 should be removed and the corresponding equivalent circuit is shown in Fig. 7a.

The corrosion of Q235 carbon steel is dramatically inhibited after adding 400 ppm N,S-CDs in 1 M HCl solution, which is evidenced by the increase in the diameter of capacitive arc and impedance modulus with immersion time (Fig. 6d and e). Although only one time constant can be seen in the phase angle-Bode plots, the corrosive behavior of steel substrate becomes complex. To better realize the corrosion process of Q235 carbon steel in the presence of 400 ppm N,S-CDs, several equivalent circuits are proposed to analyze the EIS data. As analyzed in Fig. 3b–d, the EIS data at first 3 h of immersion can be fitted with the equivalent circuit in Fig. 4. After 6 h of immersion, the active sites on Q235 carbon steel surface are partially covered with N,S-CDs, and this layer can suppress the steel surface from corrosion to some extent. Hence, the film resistance (R_f) and film capacitance (C_f) are added in the equivalent circuit, as shown in Fig. 7b. With the further extension of immersion time, the inductive loop disappears owing to the homogeneous adsorption of N,S-CDs onto the steel surface (12 h). The diffusion characteristic (Warburg impedance, W) at low frequency appears at 24 h of immersion, indicating the diffusion of corrosion medium along the formed adsorption film. Hence, the equivalent circuits in Fig. 7c and d can be used to fit the EIS data at 12 and 24 h of immersion, respectively.

Table 3 summarizes the corresponding electrochemical fitting parameters. In the blank solution, the R_{ct} value varies slightly but CPE_{dl} shows a gradual increase with the prolonged immersion time owing to the corrosion-induced increase in the surface roughness of steel. In the presence of 400 ppm N,S-CDs, R_{ct} and CPE_{dl} show the opposite variation tendency in contrast to those in the blank solution. In particular, the R_{ct} value in the presence of 400 ppm N,S-CDs is much larger than that in the blank solution. The R_{ct} value and inhibition efficiency increase while the C_{dl} value decreases with immersion time increasing from 3 h to 24 h, which is because the adsorbed water molecules on the steel surface are gradually replaced by the adsorbed N,S-CDs.[37] The maximum R_{ct}, inhibition efficiency and the corresponding C_{dl} value obtained after 24 h of immersion in the presence of 400 ppm N,S-CDs are 460.8 Ω cm^2, 95.6% and 19.81 μF cm^{-2}, respectively.

Table 3 Electrochemical fitting parameters obtained from EIS results for Q235 carbon steel after different immersion time points in 1 M HCl solution with and without 400 ppm N,S-CDs

C (ppm)	Immersion time (h)	R_s (Ω cm^2)	R_{ct} (Ω cm^2)	CPE_{dl} $Y_0 \times 10^5$ (Ω^{-1} cm^{-2} s^n)	n	C_{dl} (μF cm^{-2})	L (H cm^2)	R_L (Ω cm^2)	η (%)
Blank	3	8.16	25.28	46.6	0.91	261.00	1375	239	—
	6	8.42	22.54	92.1	0.90	531.00	2124	271.1	—
	12	8.67	22.46	152.5	0.89	886.00	7238	336.8	—
	24	8.74	26.58	242.7	0.89	1451.00	—	—	—

	Immersion time (h)	R_s (Ω cm^2)	R_{ct} (Ω cm^2)	CPE_{dl} $Y_{01} \times 10^5$ (Ω^{-1} cm^{-2} s^{n_1})	n_1	C_{dl} (μF cm^{-2})	R_f (Ω cm^2)	CPE_f $Y_{02} \times 10^5$ (Ω^{-1} cm^{-2} s^{n_2})	n_2	L (H cm^2)	R_L (Ω cm^2)	W Y_0 (Ω^{-1} cm^{-2} s$^{1/2}$)	η (%)
400	3	7.44	270.0	9.18	0.88	33.05	—	—	—	1.07×10^4	2511	—	94.6
	6	7.63	214.7	4.29	0.93	23.41	140.2	29.13	0.67	58.22	18.42	—	93.6
	12	7.87	365.2	4.13	0.92	20.51	108.6	70.46	0.77	—	—	—	95.2
	24	7.95	460.8	3.66	0.93	19.81	152.3	91.02	0.75	—	—	0.3164	95.7

Table 4 Inhibition efficiency of Q235 carbon steel after 12 h of immersion in 1 M HCl with and without 400 ppm N,S-CDs at different temperatures, as determined by the weight loss method

T (K)	C (ppm)	V_{corr} (g m^{-2} h^{-1})	η
298.15	Blank	9.1	—
	400	0.86	90.55
308.15	Blank	23	—
	400	1.8	92.17
318.15	Blank	48	—
	400	3.5	92.7
328.15	Blank	104	—
	400	6.2	94.04

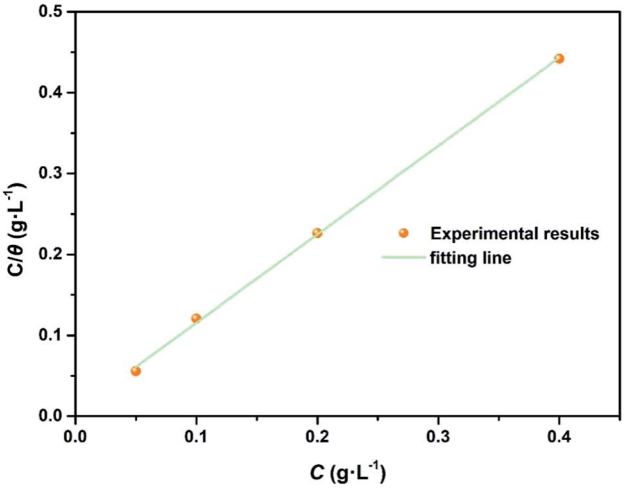

Fig. 8 Langmuir adsorption isotherm ($\frac{C_{inh}}{\theta}$ *versus* C_{inh}) of N,S-CDs in 1 M HCl at room temperature.

3.4 Adsorption isotherm

According to the above-mentioned analysis, the corrosion inhibition is mainly achieved based on the adsorption of N,S-CDs onto the steel surface. Hence, it is necessary to realize the interaction between Q235 carbon steel and N,S-CDs. In general, the adsorption of inhibitors can be divided into three types—Langmuir, Temkin and Frumkin.[5] In this investigation, compared to the latter two adsorption isotherms, Langmuir adsorption isotherm achieves the best agreement with the obtained results, which can be expressed using the following equation:[42]

$$\frac{C_{inh}}{\theta} = C_{inh} + \frac{1}{K_{ads}} \quad (6)$$

$$\theta = \eta/100 \quad (7)$$

where C_{inh} is the N,S-CD concentration, K_{ads} is defined as the adsorption equilibrium constant, and θ corresponds to the surface coverage, which can be calculated using eqn (7).

Fig. 8 presents the relationship between $\frac{C_{inh}}{\theta}$ and C_{inh}. It can be deduced from the plot intercept that the K_{ads} value is 157.73 L g^{-1}, implying the strong adsorption of N,S-CDs on the steel surface. Besides, the regression coefficient (R^2) is 0.9999, suggesting that the adsorption of N,S-CDs conforms to the Langmuir adsorption isotherm.

Ulteriorly, the adsorption free energy (ΔG^0_{ads}) of N, S-CDs was determined using the following equation:[8]

$$\Delta G^0_{ads} = -RT\ln(1000K_{ads}) \quad (8)$$

where R is the molar gas constant and T is equal to 298.15 K. Generally, ΔG^0_{ads} is used to confirm the adsorption type of corrosion inhibitor. The ΔG^0_{ads} value equal to -20 kJ mol^{-1} or more positive suggests that the electrostatic interaction exists between inhibitor molecules and steel surface, which is physisorption. In another case, the ΔG^0_{ads} value equal to -40 kJ mol^{-1} or more negative indicates the existence of the coordinate metal bond resulting from the charge transferring or sharing between N,S-CDs and steel surface, and this adsorbed type is chemisorption. The calculated ΔG^0_{ads} value by eqn (7) in this study is -29.67 kJ mol^{-1}, which falls in between -20 and -40 kJ mol^{-1}, suggesting the adsorption of N,S-CDs on the steel surface is a mixed type of physisorption and chemisorption. This result is consistent with the polarization results.

3.5 Effect of temperature

To investigate the inhibition mechanism and calculate the activation energy of the corrosion process, the corrosion

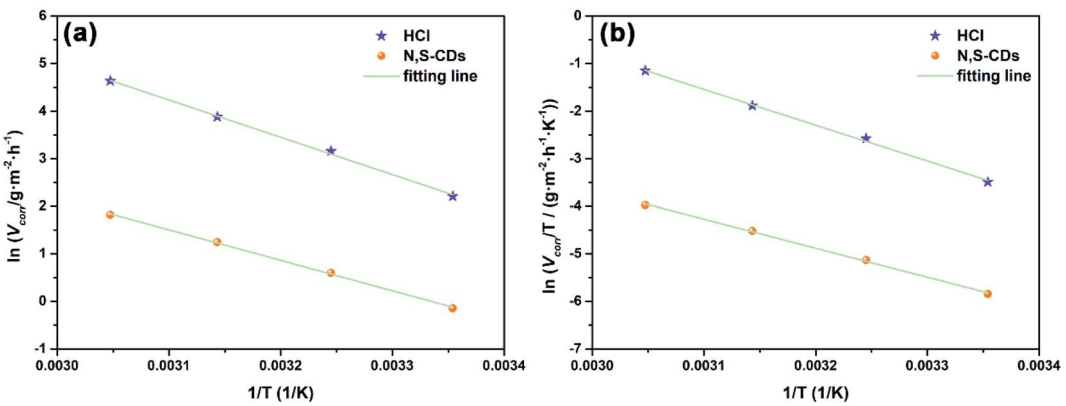

Fig. 9 (a) Arrhenius plots and (b) plots of ln V_{corr}/T *versus* $1/T$ for the corrosion of Q235 carbon steel in 1 M HCl with 400 ppm N,S-CDs.

Table 5 Activation parameters for Q235 carbon steel in 1 M HCl with and without 400 ppm N,S-CDs

C (ppm)	E_a (kJ mol^{-1})	ΔH^0 (kJ mol^{-1})	ΔS^0 (J K^{-1} mol^{-1})
Blank	65.38	62.79	−15.71
400	53.36	50.76	−75.72

inhibition performance of N,S-CDs for Q235 carbon steel was evaluated by weight loss measurement at a temperature ranging from 298.15 K to 328.15 K. The corrosion rate and inhibition efficiency in the absence and presence of 400 ppm N,S-CDs are summarized in Table 4. The corrosion rate and inhibition efficiency increase with the increase in temperature, suggesting that the adsorption of N,S-CDs onto the steel surface is primarily dominated by chemical interaction.[39]

According to the Arrhenius and transition state equation, the activation thermodynamic parameters for the corrosion process of Q235 carbon steel with and without 400 ppm N,S-CDs could be determined using the following equation:[38,43,44]

$$\ln V_{corr} = -\frac{E_a}{RT} + \ln A \quad (9)$$

$$\ln \frac{V_{corr}}{T} = \ln \frac{R}{N_A h} + \frac{\Delta S^0}{R} - \frac{\Delta H^0}{RT} \quad (10)$$

where V_{corr} is the corrosion rate of specimens, E_a is the apparent activation energy, ΔS^0 is the entropy of activation, ΔH^0 is the enthalpy of activation, T is the absolute temperature, A is the pre-exponential factor, h is Plank's constant and N_A is Avogadro's number. As shown in Fig. 9a, the plot of ln V_{corr} *versus* $1/T$ gives a linear relation and the E_a value can be calculated according to the plot slope $\left(-\frac{E_a}{R}\right)$. As shown in Table 5, the E_a value is 65.38 kJ mol^{-1} in the blank solution, which is larger than that in the presence of 400 ppm N,S-CDs (53.36 kJ mol^{-1}). The lower E_a value indicates that less active sites on the steel surface are exposed to 1 M HCl solution owing to the formation

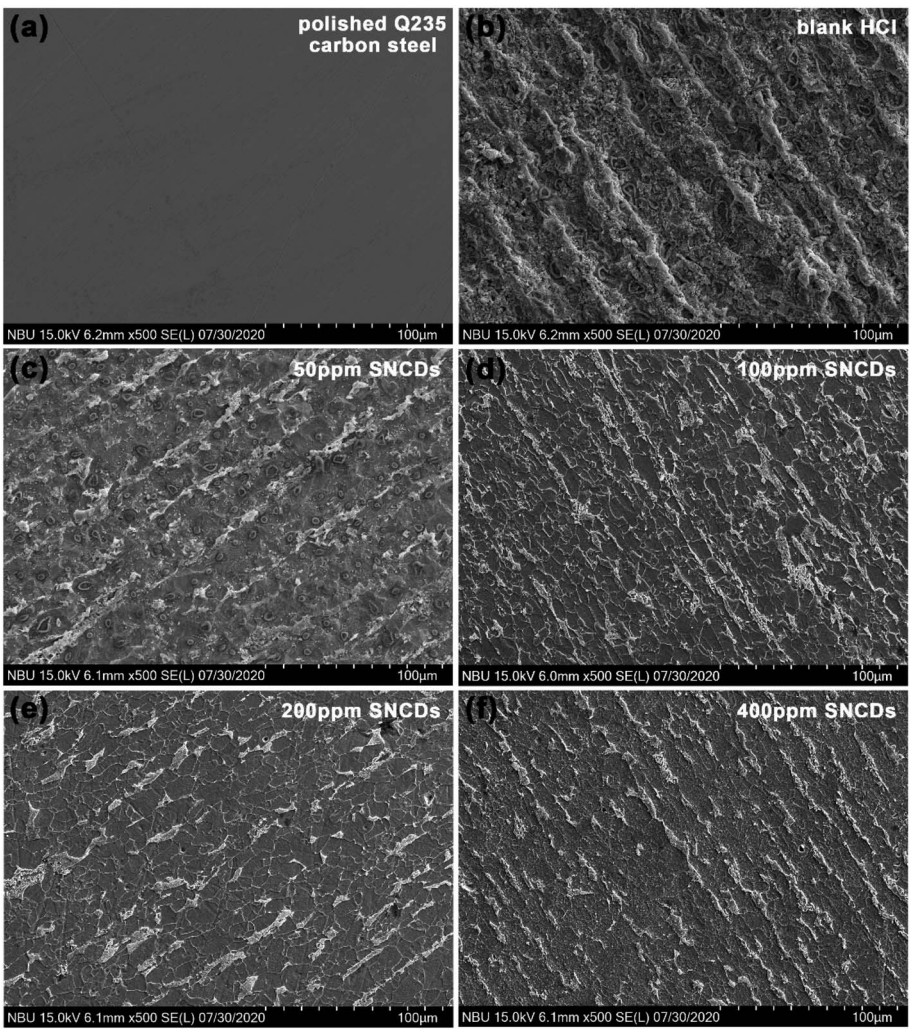

Fig. 10 SEM images of Q235 carbon steel before and after 60 h of immersion in 1 M HCl solution with and without different concentrations of N,S-CDs (a) polished Q235 carbon steel, (b) in blank HCl solution, and 1 M HCl solution with (c) 50 ppm, (d) 100 ppm, (e) 200 ppm and (f) 400 ppm of N,S-CDs.

of a protective layer of N,S-CDs.[5,36,45,46] Fig. 9b displays the plot of $\ln\frac{V_{corr}}{T}$ against $1/T$. The ΔS^0 and ΔH^0 values can be obtained from the intercept $\left(\ln\frac{R}{N_A h}+\frac{\Delta S^0}{R}\right)$ and slope $\left(-\frac{\Delta H^0}{R}\right)$ of plots. The ΔH^0 values in the blank solution and in the presence of 400 ppm N,S-CDs are 62.79 and 50.76 kJ mol^{-1}, respectively, and the positive sign of ΔH^0 implies that the dissolution of steel substrate is an endothermic process.[5] It is clear that the ΔS^0 value in the presence of 400 pm N,S-CDs (−75.72 J K^{-1} mol^{-1}) exhibits a negative increment compared to that in blank solution (−15.71 J K^{-1} mol^{-1}), indicating the formation of an orderly stable adsorption film on the steel surface.[5,36,38]

3.6 Surface analysis

For the purpose of checking the corrosion status of steel surface after immersion in the tested solutions, SEM was carried out. As shown in Fig. 10a, the polished Q235 carbon steel before immersion presents a relatively uniform and smooth surface. When Q235 carbon steel is exposed to the blank solution (Fig. 10b), the steel surface is corroded severely along the polished direction and becomes very coarse. In the presence of N,S-CDs, the corrosion of steel surface appears along the polished direction, but the corrosion degree is obviously inhibited with the increase in N,S-CD concentration.

Subsequently, the surface roughness (RSa) of the steel substrate was characterized using SPM. As presented in Fig. 11, the RSa value is 0.27 μm for the polished Q235 carbon steel. After immersion in the blank solution, the steel surface experiences a severe corrosion, leading to a remarkable increase in the RSa value (1.87 μm). In case of the presence of N,S-CDs, the RSa value decreases significantly compared with that in blank solution, and varies from 0.87 μm to 0.60 μm with the increase in N,S-CD concentration, which agrees well with the above-mentioned SEM results, proving that the addition of N,S-CDs can provide effective protection for Q235 carbon steel in 1 M HCl solution.

The adsorption kinetics of N,S-CDs on the Q235 carbon steel surface was also analyzed by XPS. It is clear from Fig. 12a that after 60 h of immersion in the presence of 400 ppm N,S-CDs, N and S elements are detected from the steel surface, and the elemental composition of steel surface mainly includes C (30.03 wt%), O (29.02 wt%), N (1.41 wt%), S (1.28 wt%), and Fe (38.26 wt%), indicating the adsorption of N,S-CDs onto the steel surface. The high-resolution spectra for various elements are further analyzed and shown in Fig. 12b–f. For the C 1 s spectrum (Fig. 12b), three peaks located at 284.6, 286.1 and 288.3 eV, are attributed to sp^2 C (C=C), sp^3 C (C–N, C–O and C–S), and C=O/C=S/C=N, respectively.[47] The O 1s spectrum exhibits three peaks at 529.7, 531.1 and 532.1 eV which correspond to the existence of Fe_2O_3, C=O and C–O, respectively (Fig. 12c). In case of the N 1s spectrum, the peaks at 399.5 and 400.4 eV are assigned to the pyridinic N and pyrrolic N, respectively (Fig. 12d).[42,47] Different with the N 1s spectrum of N,S-CDs, a peak appears at 398.3 eV, which may be attributed to the coordinated N.[48] For the S 2p spectrum in Fig. 12e, the peaks at 161.9 and 163.2 eV are related to the S–Fe and C–S/C=S bonds, respectively.[25] Besides, the Fe 2p$^{3/2}$ spectrum in Fig. 12f can be divided into three peaks at 712.3, 710.9 and 710.0 eV that are

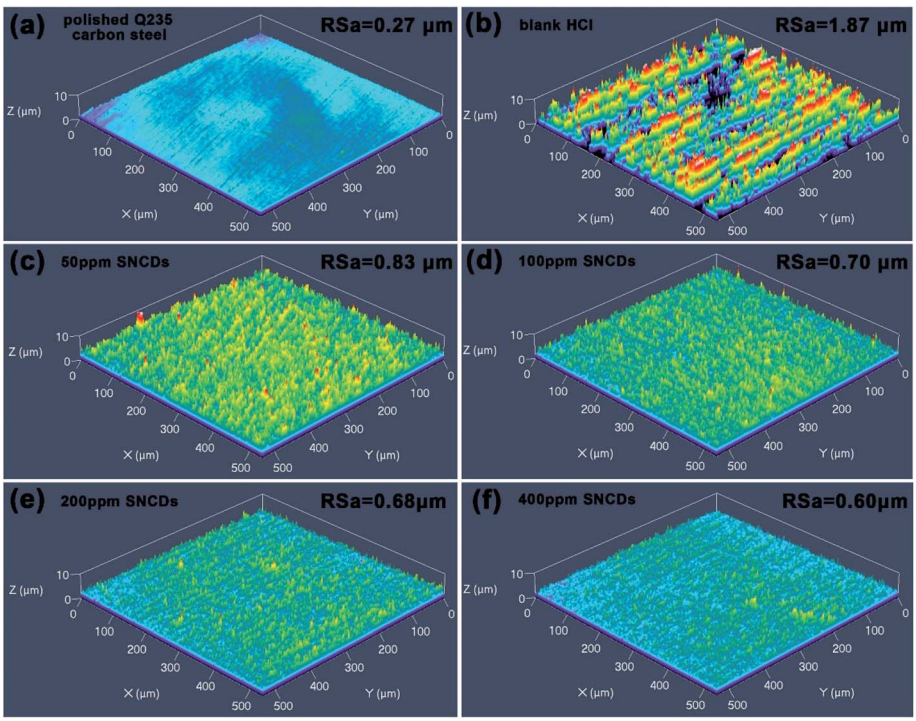

Fig. 11 SPM images of Q235 carbon steel before and after 60 h of immersion in 1 M HCl solution with and without different concentrations of N,S-CDs (a) polished Q235 carbon steel, (b) in 1 M HCl solution, and 1 M HCl solution with (c) 50 ppm, (d) 100 ppm, (e) 200 ppm and (f) 400 ppm N,S-CDs.

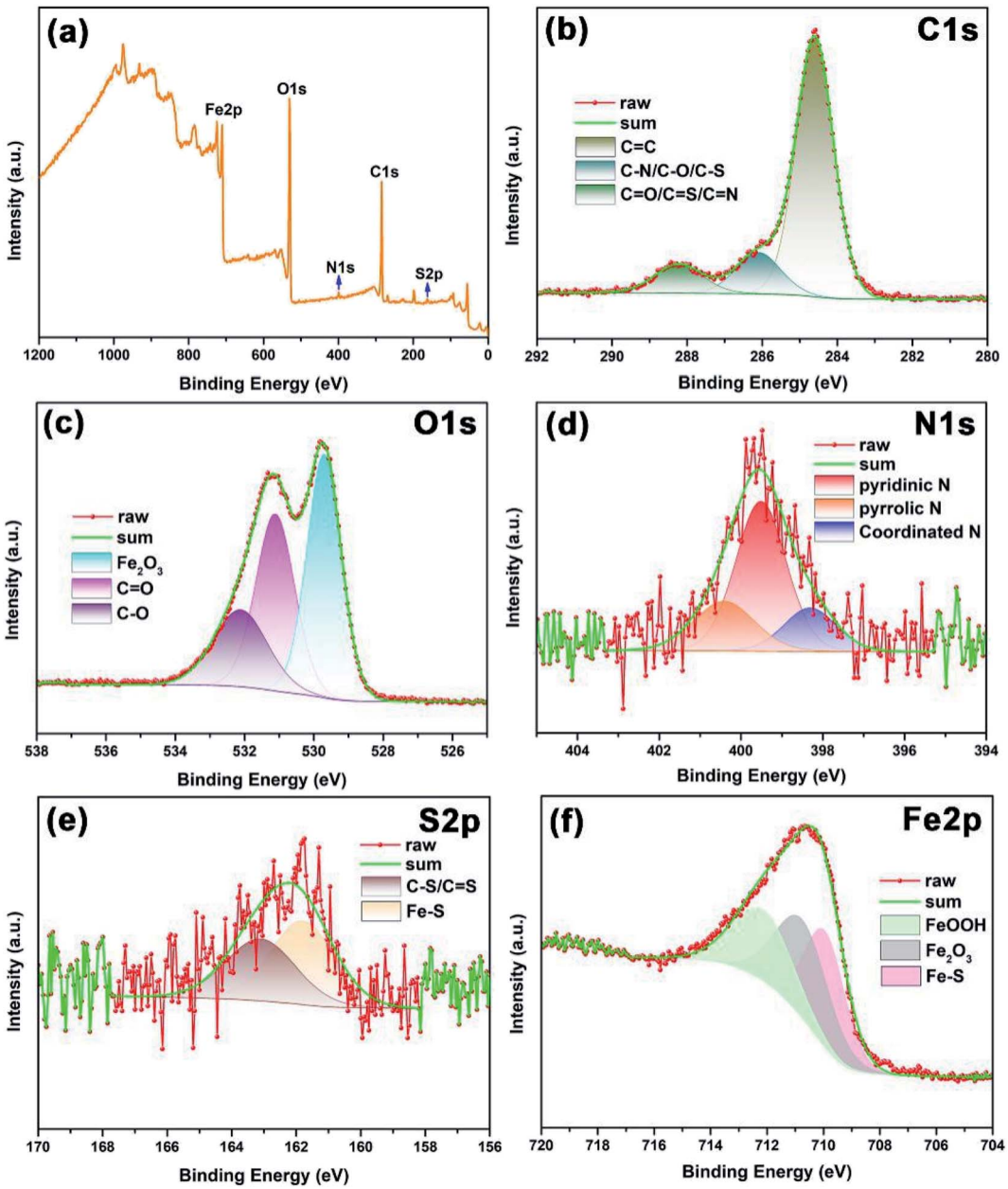

Fig. 12 (a) Full-range XPS spectrum of Q235 carbon steel with 400 ppm of N,S-CDs, and the corresponding high-resolution XPS spectra of (b) C 1s, (c) O 1s, (d) N 1s, (e) S 2p, and (f) Fe 2p.

attributed to FeOOH, Fe_2O_3, and Fe–S, respectively, which is consistent with the Fe_2O_3 peak in the O 1s spectrum and the Fe–S peak in the S 2p spectrum.[25,49,50] The formation of the peak of coordinated N and Fe–S suggests the chemisorption adsorption of N, S-CDs on Q235 carbon steel.

3.7 Inhibition mechanism

Based on the above-mentioned analysis of experimental results, a possible model could be proposed to illustrate the inhibition mechanism of N,S-CDs. It is well recognized that the adsorption of inhibitor molecules onto the metal surface is always realized by replacing the adsorbed water molecules. In the blank solution, N,S-CDs become protonated in equilibrium owing to the presence of nitrogen atoms. Besides, the steel surface always carries a positive excess charge in the HCl solution.[36,41] As illustrated in Fig. 13a, the hydrated chloride ions can be specifically adsorbed onto the steel surface with positive charges *via* electrostatic interaction, which can act as interconnecting bridges to favor the adsorption of protonated N,S-CDs on the positively charged steel surface.[41] Then, protonated N,S-CDs adsorbed onto the steel surface would compete with hydrogen ions, thus reducing the reaction rate of hydrogen evolution. In addition to physisorption, it is observed from the FTIR and XPS results that the heteroatoms (N and S) in N,S-CDs exist in the form of single and multiple bonds, which will make the N,S-CDs easily adsorb onto the steel surface by forming lone pair electrons and coordinated bonds with Fe

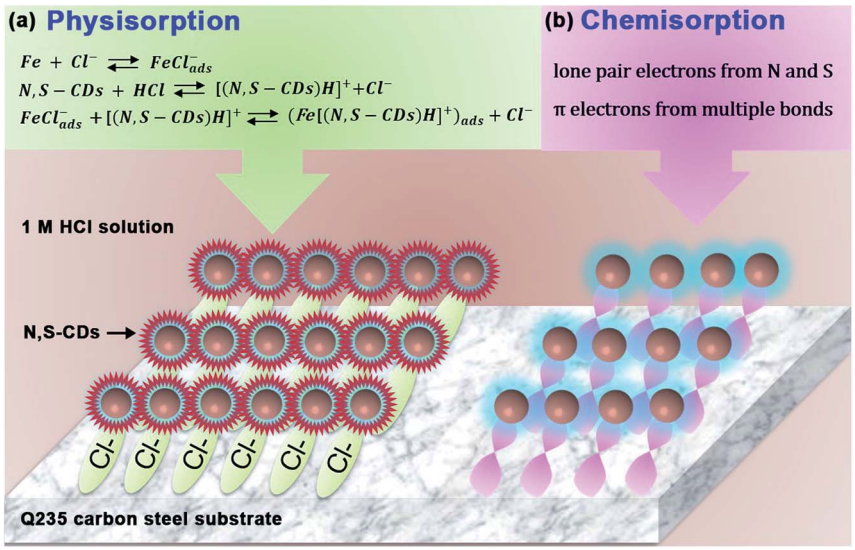

Fig. 13 Inhibition mechanism of N,S-CDs on the Q235 carbon steel surface in 1 M HCl solution.

atoms (Fig. 13b). Thus, N,S-CDs could effectively prevent Q235 carbon steel from acid corrosion.

4. Conclusions

In this study, N,S-CDs have been prepared as novel eco-friendly corrosion inhibitors by a hydrothermal method. Systematically experimental measurements were carried out to study the corrosion inhibition performance of N,S-CDs for Q235 carbon steel in 1 M HCl solution, and the conclusions are summarized as follows:

(1) Electrochemical and weight loss results revealed that N,S-CDs could act as effective corrosion inhibitors to protect Q235 carbon steel from corrosion in 1 M HCl solution. Moreover, the inhibition efficiency increased with the increase in N,S-CD concentration and reached up to 96.6% in the presence of 400 ppm N,S-CDs.

(2) The adsorption of N,S-CDs onto the steel surface involved both physisorption and chemisorption, and conformed to the Langmuir adsorption model.

(3) The inhibition efficiency of N,S-CDs increased with the temperature ranging from 298 K to 318 K although the rising temperature accelerated the corrosion process of Q235 carbon steel.

(4) The excellent inhibitory effect of N,S-CDs was also confirmed by the decrease in the corrosion and surface roughness of Q235 carbon steel.

(5) XPS results further verified the adsorption of N,S-CDs onto the steel surface, which was attributed to the formation of lone pair electrons and coordinated bonds.

Conflicts of interest

The authors declare that they have no known competing financial interests or personal relationships that could have appeared to influence the work reported in this paper.

Acknowledgements

The authors gratefully acknowledged the financial support provided by National Natural Science Foundation of China (No. 51905278) and the Special research funding from the Marine Biotechnology and Marine Engineering Discipline Group in Ningbo University.

References

1 A. Farhadian, A. Rahimi, N. Safaei, *et al.*, A theoretical and experimental study of castor oil-based inhibitor for corrosion inhibition of mild steel in acidic medium at elevated temperatures, *Corros. Sci.*, 2020, 175.

2 C. Liang, Z. Liu, Q. Liang, *et al.*, Synthesis of 2-aminofluorene bis-Schiff base and corrosion inhibition performance for carbon steel in HCl, *J. Mol. Liq.*, 2019, **277**, 330–340.

3 M. A. Bedair, M. M. B. El-Sabbah, A. S. Fouda, *et al.*, Synthesis, electrochemical and quantum chemical studies of some prepared surfactants based on azodye and Schiff base as corrosion inhibitors for steel in acid medium, *Corros. Sci.*, 2017, **128**, 54–72.

4 Y. Qiang, S. Zhang, B. Tan, *et al.*, Evaluation of Ginkgo leaf extract as an eco-friendly corrosion inhibitor of X70 steel in HCl solution, *Corros. Sci.*, 2018, **133**, 6–16.

5 M. Behpour, S. M. Ghoreishi, N. Soltani, *et al.*, The inhibitive effect of some bis-N,S-bidentate Schiff bases on corrosion behaviour of 304 stainless steel in hydrochloric acid solution, *Corros. Sci.*, 2009, **51**(5), 1073–1082.

6 L. L. Liao, S. Mo, H. Q. Luo, *et al.*, Longan seed and peel as environmentally friendly corrosion inhibitor for mild steel in acid solution: Experimental and theoretical studies, *J. Colloid Interface Sci.*, 2017, **499**, 110–119.

7 A. Dehghani, G. Bahlakeh, B. Ramezanzadeh, *et al.*, A combined experimental and theoretical study of green corrosion inhibition of mild steel in HCl solution by

aqueous Citrullus lanatus fruit (CLF) extract, *J. Mol. Liq.*, 2019, **279**, 603–624.

8 P. Mourya, S. Banerjee and M. M. Singh, Corrosion inhibition of mild steel in acidic solution by Tagetes erecta (Marigold flower) extract as a green inhibitor, *Corros. Sci.*, 2014, **85**, 352–363.

9 H. Ding, S. B. Yu, J. S. Wei, *et al.*, Full-Color Light-Emitting Carbon Dots with a Surface-State-Controlled Luminescence Mechanism, *ACS Nano*, 2016, **10**(1), 484–491.

10 W. Lu, X. Gong, M. Nan, *et al.*, Comparative study for N and S doped carbon dots: Synthesis, characterization and applications for Fe(3+) probe and cellular imaging, *Anal. Chim. Acta*, 2015, **898**, 116–127.

11 S. S. Monte-Filho, S. I. E. Andrade, M. B. Lima, *et al.*, Synthesis of highly fluorescent carbon dots from lemon and onion juices for determination of riboflavin in multivitamin/mineral supplements, *J. Pharm. Anal.*, 2019, **9**(3), 209–216.

12 M. Cui, S. Ren, Q. Xue, *et al.*, Carbon dots as new eco-friendly and effective corrosion inhibitor, *J. Alloys Compd.*, 2017, **726**, 680–692.

13 M. Cui, S. Ren, H. Zhao, *et al.*, Novel nitrogen doped carbon dots for corrosion inhibition of carbon steel in 1 M HCl solution, *Appl. Surf. Sci.*, 2018, **443**, 145–156.

14 Y. Qiang, S. Zhang, H. Zhao, *et al.*, Enhanced anticorrosion performance of copper by novel N-doped carbon dots, *Corros. Sci.*, 2019, 161.

15 Y. Ye, D. Yang, H. Chen, *et al.*, A high-efficiency corrosion inhibitor of N-doped citric acid-based carbon dots for mild steel in hydrochloric acid environment, *J. Hazard. Mater.*, 2019, **381**, 121019.

16 Y. Ye, Y. Zou, Z. Jiang, *et al.*, An effective corrosion inhibitor of N doped carbon dots for Q235 steel in 1 M HCl solution, *J. Alloys Compd.*, 2020, 815.

17 Y. Ye, D. Yang and H. Chen, A green and effective corrosion inhibitor of functionalized carbon dots, *J. Mater. Sci. Nanotechnol.*, 2019, **35**(10), 2243–2253.

18 P. A. Denis, Lithium adsorption on heteroatom mono and dual doped graphene, *Chem. Phys. Lett.*, 2017, **672**, 70–79.

19 P. A. Denis and C. P. Huelmo, Structural characterization and chemical reactivity of dual doped graphene, *Carbon*, 2015, **87**, 106–115.

20 P. A. Denis, C. P. Huelmo and F. Iribarne, Theoretical characterization of sulfur and nitrogen dual-doped graphene, *Comput. Theor. Chem.*, 2014, **1049**, 13–19.

21 S. Ullah, P. A. Denis and F. Sato, Unusual Enhancement of the Adsorption Energies of Sodium and Potassium in Sulfur–Nitrogen and Silicon–Boron Codoped Graphene, *ACS Omega*, 2018, **3**, 15821–15828.

22 V. Saraswat and M. Yadav, Carbon Dots as Green Corrosion Inhibitor for Mild Steel in HCl Solution, *ChemistrySelect*, 2020, **5**(25), 7347–7357.

23 H. Cen, Z. Chen and X. Guo, N,S co-doped carbon dots as effective corrosion inhibitor for carbon steel in CO_2-saturated 3.5% NaCl solution, *J. Taiwan Inst. Chem. Eng.*, 2019, **99**, 224–238.

24 H. Cen, X. Zhang, L. Zhao, *et al.*, Carbon dots as effective corrosion inhibitor for 5052 aluminium alloy in 0.1 M HCl solution, *Corros. Sci.*, 2019, 161.

25 D. Guo, H.-F. Wei, R.-B. Song, *et al.*, N,S-doped carbon dots as dual-functional modifiers to boost bio-electricity generation of individually-modified bacterial cells, *Nano Energy*, 2019, **63**, 103875.

26 E. N. Suciu, B. Kuhlmann, G. A. Knudsen, *et al.*, Investigation of dialkyltin compounds as catalysts for the synthesis of dialkyl carbonates from alkyl carbamates, *J. Organomet. Chem.*, 1998, **556**, 41–54.

27 Z. Qin, W. Wang, X. Zhan, *et al.*, One-pot synthesis of dual carbon dots using only an N and S co-existed dopant for fluorescence detection of Ag(+), *Spectrochim. Acta, Part A*, 2019, **208**, 162–171.

28 P. Zuo, J. Liu, H. Guo, *et al.*, Multifunctional N,S co-doped carbon dots for sensitive probing of temperature, ferric ion, and methotrexate, *Anal. Bioanal. Chem.*, 2019, **411**(8), 1647–1657.

29 P. Zhu, D. Lyu, P. K. Shen, *et al.*, Sulfur-rich carbon dots as a novel fluorescent imaging probe for distinguishing the pathological changes of mouse-bone cells, *J. Lumin.*, 2019, **207**, 620–625.

30 C. Sun, Y. Zhang, P. Wang, *et al.*, Synthesis of Nitrogen and Sulfur Co-doped Carbon Dots from Garlic for Selective Detection of Fe(3+), *Nanoscale Res. Lett.*, 2016, **11**(1), 110.

31 Y. Dong, H. Pang, H. B. Yang, *et al.*, Carbon-Based Dots Co-doped with Nitrogen and Sulfur for High Quantum Yield and Excitation-Independent Emission, *Angew. Chem., Int. Ed.*, 2013, **52**(30), 7800–7804.

32 D. Sun, R. Ban, P.-H. Zhang, *et al.*, Hair fiber as a precursor for synthesizing of sulfur- and nitrogen-co-doped carbon dots with tunable luminescence properties, *Carbon*, 2013, **64**, 424–434.

33 E. B. Ituen, O. Akaranta and S. A. Umoren, N-acetyl cysteine based corrosion inhibitor formulations for steel protection in 15% HCl solution, *J. Mol. Liq.*, 2017, **246**, 112–118.

34 P. Singh, D. S. Chauhan, S. S. Chauhan, *et al.*, Chemically modified expired Dapsone drug as environmentally benign corrosion inhibitor for mild steel in sulphuric acid useful for industrial pickling process, *J. Mol. Liq.*, 2019, 286.

35 B. Tan, S. Zhang, H. Liu, *et al.*, Corrosion inhibition of X65 steel in sulfuric acid by two food flavorants 2-isobutylthiazole and 1-(1,3-Thiazol-2-yl) ethanone as the green environmental corrosion inhibitors: Combination of experimental and theoretical researches, *J. Colloid Interface Sci.*, 2019, **538**, 519–529.

36 A. Khadiri, R. Saddik, K. Bekkouche, *et al.*, Gravimetric, electrochemical and quantum chemical studies of some pyridazine derivatives as corrosion inhibitors for mild steel in 1 M HCl solution, *J. Taiwan Inst. Chem. Eng.*, 2016, **58**, 552–564.

37 J. Aljourani, K. Raeissi and M. A. Golozar, Benzimidazole and its derivatives as corrosion inhibitors for mild steel in 1M HCl solution, *Corros. Sci.*, 2009, **51**(8), 1836–1843.

38 C. M. Fernandes, T. d. S. Ferreira Fagundes, N. Escarpini dos Santos, *et al.*, Ircinia strobilina crude extract as corrosion

inhibitor for mild steel in acid medium, *Electrochim. Acta*, 2019, **312**, 137–148.

39 A. Dehghani, G. Bahlakeh, B. Ramezanzadeh, *et al.*, Potential of Borage flower aqueous extract as an environmentally sustainable corrosion inhibitor for acid corrosion of mild steel: Electrochemical and theoretical studies, *J. Mol. Liq.*, 2019, **277**, 895–911.

40 A. Ehsani, M. G. Mahjani, M. Hosseini, *et al.*, Evaluation of Thymus vulgaris plant extract as an eco-friendly corrosion inhibitor for stainless steel 304 in acidic solution by means of electrochemical impedance spectroscopy, electrochemical noise analysis and density functional theory, *J. Colloid Interface Sci.*, 2017, **490**, 444–451.

41 M. M. Solomon, S. A. Umoren, M. A. Quraishi, *et al.*, Myristic acid based imidazoline derivative as effective corrosion inhibitor for steel in 15% HCl medium, *J. Colloid Interface Sci.*, 2019, **551**, 47–60.

42 M. Tourabi, K. Nohair, M. Traisnel, *et al.*, Electrochemical and XPS studies of the corrosion inhibition of carbon steel in hydrochloric acid pickling solutions by 3,5-bis(2-thienylmethyl)-4-amino-1,2,4-triazole, *Corros. Sci.*, 2013, **75**, 123–133.

43 L. L. Liao, S. Mo, J. L. Lei, *et al.*, Application of a cosmetic additive as an eco-friendly inhibitor for mild steel corrosion in HCl solution, *J. Colloid Interface Sci.*, 2016, **474**, 68–77.

44 X. Zheng, S. Zhang, W. Li, *et al.*, Experimental and theoretical studies of two imidazolium-based ionic liquids as inhibitors for mild steel in sulfuric acid solution, *Corros. Sci.*, 2015, **95**, 168–179.

45 D. B. Hmamou, R. Salghi, A. Zarrouk, *et al.*, Weight Loss, Electrochemical, Quantum Chemical Calculation, and Molecular Dynamics Simulation Studies on 2-(Benzylthio)-1,4,5-triphenyl-1H-imidazole as an Inhibitor for Carbon Steel Corrosion in Hydrochloric Acid, *Ind. Eng. Chem. Res.*, 2013, **52**(40), 14315–14327.

46 C. M. Fernandes, L. X. Alvarez, N. E. dos Santos, *et al.*, Green synthesis of 1-benzyl-4-phenyl-1*H*-1,2,3-triazole, its application as corrosion inhibitor for mild steel in acidic medium and new approach of classical electrochemical analyses, *Corros. Sci.*, 2019, **149**, 185–194.

47 T. Liu, Z. W. Cui, J. Zhou, *et al.*, Synthesis of Pyridinic-Rich N, S Co-doped Carbon Quantum Dots as Effective Enzyme Mimics, *Nanoscale Res. Lett.*, 2017, **12**(1), 375.

48 A. Zarrouk, B. Hammouti, T. Lakhlifi, *et al.*, New 1 H -pyrrole-2,5-dione derivatives as efficient organic inhibitors of carbon steel corrosion in hydrochloric acid medium: Electrochemical, XPS and DFT studies, *Corros. Sci.*, 2015, **90**, 572–584.

49 G. A. Zhang, D. Liu, Y. Z. Li, *et al.*, Corrosion behaviour of N80 carbon steel in formation water under dynamic supercritical CO_2 condition, *Corros. Sci.*, 2017, **120**, 107–120.

50 H. Liu, T. Gu, Y. Lv, *et al.*, Corrosion inhibition and anti-bacterial efficacy of benzalkonium chloride in artificial CO_2-saturated oilfield produced water, *Corros. Sci.*, 2017, **117**, 24–34.